VOL. 18, NO. 8, APRIL 2023 ISSN 1819-6608
ARPN Journal of Engineering and Applied Sciences

www.arpnjournals.com

EXPERIMENTAL AND PARAMETRIC ANALYSIS OF EXHAUST HEAT EXCHANGER USED IN THERMOELECTRIC GENERATOR

Dipak S. Patil
Department of Mechanical Engineering, G H Raisoni College of Engineering and Management, Wagholi, Pune, India
E-Mail: dspatil100@gmail.com

ABSTRACT

A thermoelectric generator system consists of an exhaust heat exchanger, a thermoelectric module, and water heat exchanger. Perfect heat exchangers recover as much heat energy as possible from engine exhaust with an acceptable pressure drop. The capacity and efficiency of the heat exchanger depend on its shape, type, and material of the heat exchanger. The main objective of this research was to perform a parametric analysis of the test section of the exhaust heat exchanger by using simulation tools. The simulation results were validated with the experimental results to ensure the performance of the simulation model. The performance of the test section was measured in relation to geometry, pressure drop, temperature distribution, fluid velocity, and temperature uniformity coefficient. The test section of 60 mm × 60 mm × 180 mm (F-type) shows a higher surface temperature with an allowable pressure drop than the other types of test section without inserts. The inserts played a vital role in enhancing the surface temperature distribution and uniformity coefficient. The cone type (G-type), cone-cylinder type (H-type), and cone-cylinder-cone type (I-type) inserts were used to improve the performance of the F-type test section. The G-type and H-type test sections of the exhaust heat exchanger have a high surface temperature, high-temperature uniformity, and allowable pressure drop.

Keywords: computational fluid dynamic, exhaust heat exchanger, heat transfer coefficient, thermoelectric generator.

Manuscript Received 11 January 2023; Revised 22 May 2023; Published 15 June 2023

INTRODUCTION

According to the basic concepts and background of the thermoelectric system, it is observed that a thermoelectric module (TEM) is fixed between the heat source and the heat sink. The heat source and sink create a temperature difference on both sides of the thermoelectric module, which is essential to generate electric power. The design of heat exchangers and thermoelectric module selection is very vital for thermoelectric generator (TEG) systems. Researchers are currently concentrating on the design and development of thermoelectric generator systems and heat exchangers (HE). New TEG parameters, such as the number of TEMs, cooling systems, heat exchangers and the thermoelectric materials, should be optimized. The size and shape of the heat exchanger and number of thermoelectric couples govern the thermoelectric output power (WengChien-Chou *et al*., 2013). The conversion efficiency and power output of the TEG are significantly affected by the heat source temperature and the mass flow rate of the fluids (PatilDipak S *et al*., 2018). More effective heat exchangers extract large amounts of heat from vehicle exhaust with an allowable drop in pressure. Heat exchangers supply preliminary heat for a TEG, and their efficiency and capacity are affected by the heat exchanger type, material and shape (Bai Shengqiang *et al*., 2014; PatilDipak S. *et al*., 2018). The performance of the TEG was affected by the heat capacity and heat transfer of the heat recovery device. More thermoelectric modules are required to increase the output power of the TEG, which requires a large surface area. Therefore, the weight and size of the heat exchanger has increased. The optimization of exhaust the heat exchanger surface area is a different type of issue than internal structures. (Su C.Q. *et al*., 2014). The plate-shaped exhaust heat exchanger (EHE) is suitable for thermoelectric generators because of the short distance between the ground and automobile chassis. Different types of inserts, fin structures and heat exchanger configurations are used to enhance the heat transfer (Tzeng Sheng-Chung *et al*., 2014; AmaralCalil *et al*., 2014; Kim Tae Young *et al*., 2016). The heat transfer rate of the heat exchanger is improved by using metal foam in the channel of the fluid flow because it has a larger surface area per unit volume and more contact when fluid flows through the foam of the metal (Wang Tongcai *et al*., 2014). The fin number increases the heat source temperature but the fin thickness increases the pressure drop because of the reduction in the cross-section area of the flow channel (Kim Tae Young *et al*., 2016). Kumar C. Ramesh *et al*. (2011) used computational fluid dynamic (CFD) code to develop computer-aided design and heat exchanger analysis for fluid flow and heat transfer performance. The fluid flow through the heat exchanger was assumed unsteady and turbulent. An iterative algorithm was used to resolve the governing equations. Deng Y. D. *et al*. (2013) developed a 3-dimensional heat exchanger model with internal structures. The analysis and simulation of exhaust flows through heat exchangers were performed using computational fluid dynamics software. The standard k-omega model was used for the CFD simulation. It was considered to have a fully turbulent flow and negligible viscosity. The pressure at the exit of the heat exchanger was atmospheric pressure. The heat transfer coefficient by convection between the heat exchanger surface and air was considered 20 W/m^{2}K. The design of a heat exchanger with various internal structures,

CFD analysis, and experimentation were performed by Su C. Q. *et al*. (2012). A CFD tool was applied to simulate the temperature distribution of the exhaust flowing through the heat exchanger. The desired thermal simulation was performed by varying the internal structure of the heat exchanger. For the CFD analysis and simulation, some assumptions were made that the fluid is incompressible, with negligible molecular viscosity, and fully turbulent fluid flow. The turbulent model k-ε was used for simulation purposes. The boundary conditions are very important for the simulation, such as the fluid inlet temperature, fluid velocity, exit back pressure of the system, and convection heat transfer between the heat exchanger surface and air. Su C. Q. *et al*. (2014) attempted to achieve a higher temperature at the interface and uniform temperature distribution through different types of internal structures, such as fishbone, scatter, and accordion shape. The accordion and fishbone structures have a higher temperature at the interface than the scatter structures. The accordion-shaped structure showed a more uniform temperature distribution than other structures. Based on temperature distribution, the accordion shape is more appropriate for thermoelectric generators. Liu X. *et al.* (2014) performed a CFD simulation and analysis of a heat exchanger with chaos and fishbone shaped structures. The turbulence model, κ–ε, was used for the computational fluid dynamic analysis. For all solid walls, no-slip boundary conditions were considered. The fluid flow velocity and temperature at the inlet were considered as the boundary conditions. Bai Shengqiang *et al.* (2014) developed a heat exchanger with different internal structures such as an inclined plate, parallel plate, separate plate with holes, series plate and novel pipe structures, and a CFD model was used to compare the pressure drop and heat transfer. Heat exchange with a symmetrical dimple arrangement in the upper and lower surfaces of the heat exchange was developed by Wang Yiping *et al*. (2016) to improve the rate of heat transfer with a smaller drop in pressure. Tang Z. B. *et al*. (2015) carried out an analysis of thermal uniformity; it includes index parameters, such as the coefficient of temperature or thermal uniformity γ, which are used to determine temperature uniformity. Equation 1 was used to determine the temperature uniformity of the surface:

$$\gamma = 1 - \frac{1}{\sqrt{x}} \sum_{i=1}^{x} \frac{\sqrt{(T_i - T_m)^2}}{T_m} \quad (1)$$

Where, x is the number of thermocouples, T_i is the probed temperature at i position and T_m represents the heat exchanger surface temperature. The coefficient of thermal uniformity (γ) fluctuates from 0 to 1. When γ =1 it shows that the temperature is constant throughout the surface.

The above review shows that the exhaust heat exchanger is a key component of the thermoelectric generator. The performance of the thermoelectric generator depends critically on the design of the exhaust heat exchanger. Simulation tools such as computational fluid dynamics can be used for the parametric analysis of the exhaust heat exchanger. The simulation results should be matched with the experimental results to ensure that the simulation tool can be used for further parametric analyses of the thermal system. Different types of inserts enhance the performance of the exhaust heat exchanger and obviously enhance the performance of the thermoelectric generator.

EXPERIMENTATION

The aim of the experiment was to determine the surface temperature of the test section and check the temperature uniformity. An ideal heat exchanger should have a high surface temperature and temperature uniformity coefficient. The thermal stress on the hot surface of the duct can be reduced by maintaining a higher thermal uniformity. An experimental system was developed for the exhaust heat exchanger.

Figures 1 and 2 show the layout and a photograph of the experiment setup, respectively. The experimental setup consisted of an engine setup, exhaust heat exchanger, type K thermocouples, U-tube manometer, and temperature meter/indictor. The test section (duct) of 80 × 80 mm cross-section with a length of 300 mm was made up of a 3 mm thick aluminum sheet. The thin aluminum sheet was used to reduce the thermal resistance and increase the heat transfer rate.

The outer and inner surface temperatures of the duct are the same to be considered because of the higher thermal conductivity of the thin aluminum sheets. The exhaust of an engine running at a full-load condition of 10 kg was used as the heat source. The flow rate of the engine exhaust is the sum of the air and fuel flow rates used in the engine. This information was obtained from the data acquisition system of the engine. The mass flow rate of the air and fuel were 1.05 and 28.19 kg/hr. respectively. The total exhaust flow rate was 0.00812 kg/s at the full load condition of the engine.

The exhaust temperatures were measured using cartage-type thermocouples fixed at the entry and exit of the duct. All the outer surface temperatures of the duct were measured using twenty numbers of Type-K thermocouples (T1 to T20) with temperature meter. During the experiment ambient temperature was 28^{o}C. The exhaust temperatures at the inlet and outlet of the duct were measured using thermocouples T21 and T22 at 280.5^{o}C and 195.0^{o}C respectively.

A pressure drop in the duct was measured by using 'U'- tube manometer in terms of the water column and it was 196.2 Pa. The average surface temperatures of the duct obtained during experimentation were 137.62, 136, 132, 124.06 and 115,75^{o}C along the lengths of ducts 0, 75, 150, 225, and 300 mm respectively and as shown in Figure-3.

The temperature uniformity coefficient calculated using Equation 1 was 0.87. The average exhaust temperatures at the entry and exit of the duct were 280.5

and 196.5°C, and the pressure drop of the system was 196.2 Pa.

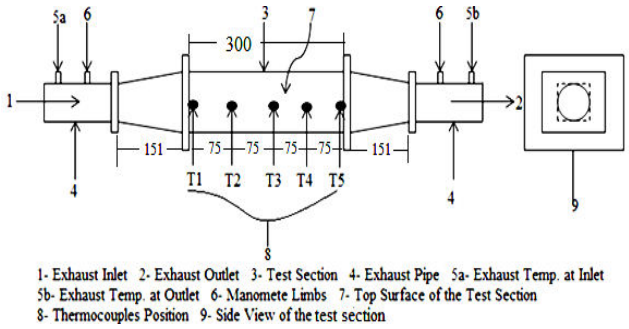

Figure-1. Schematic layout of the experimental setup of duct (80× 80×300 mm) assembly.

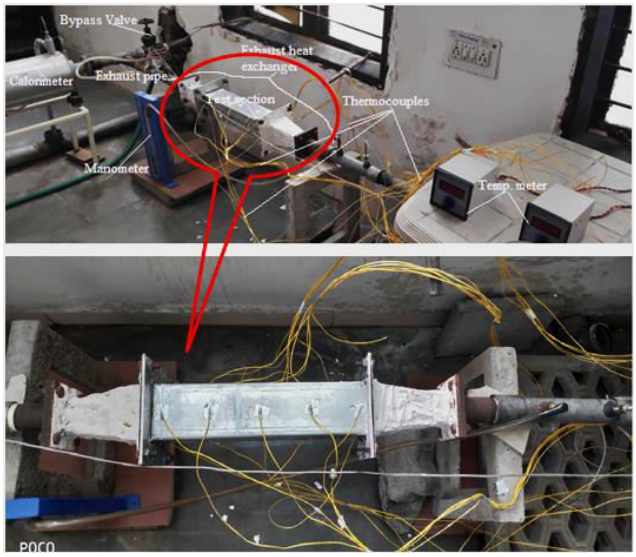

Figure-2. Photograph of experimental setup of duct (80× 80×300 mm).

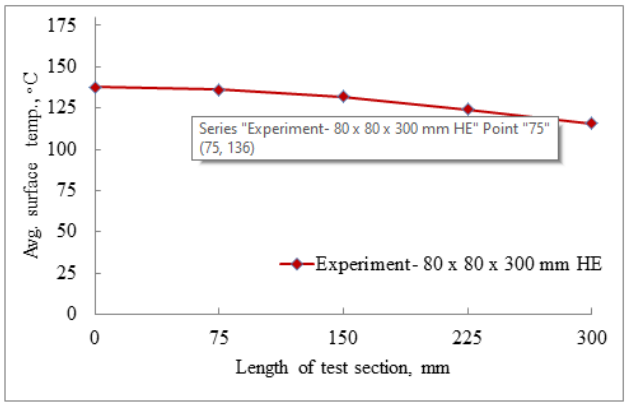

Figure-3. Surface temperature varies with length of the test section.

HEAT EXCHANGER- THERMAL SIMULATION

The simulation tool can be used for the parametric analysis of the test section because it reduces the cost and quality time. Therefore, the simulation results of the test section (80 mm × 80 mm × 300 mm) of the exhaust heat exchanger should be verified using experimental results.

The surface thermal distribution of the exhaust heat exchanger is essential in various aspects, as follows:

- It determined the operating temperature for selecting thermoelectric module material.
- It affected the conversion efficiency of heat energy to electrical energy and
- It dominated the thermal stress uniformity in module and device level.

The rough surface contact between the heat exchanger and thermoelectric module can be caused by non-uniform temperature distribution, resulting in permanent damage to the thermo-electric generator modules (Liu X., *et al.*, 2014). Typical software, the computational fluid dynamic was used to simulate the exhaust gas flow through the EHE, enabling the simulation of the surface temperature distribution. The ideal or best results of the thermal field simulation can be achieved by varying the cross-sectional area and length of the EHE and introducing different types of inserts into the test section of the heat exchanger.

Model Description

As the main element of the TEG, the exhaust heat exchanger acts as a heat source to recover the waste heat from the engine exhaust and provides TEMs for energy conversion with the help of a heat sink (coolant). In the present study, a simple numerical model of an exhaust heat exchanger without a heat sink and its effects on the thermal equilibrium process were considered. It was simulated by setting a heat transfer coefficient by convection between the heat exchanger surface and the ambient environment.

Geometric Configuration

As shown in Figure-4, the 3D model of the exhaust heat exchanger was divided into the inlet, front, middle, rear and outlet parts. The Cartesian coordinates (X, Y, and Z) of the system were fixed. A schematic layout of the exhaust heat exchanger is shown in figure 5. The inlet and outlet of the exhaust heat exchanger is a cylindrical pipe of 38 mm inlet diameter with 5 mm thick of Galvanized Iron (G. I.) material. The front part of the exhaust heat exchanger has a cross-section of 38 × 38 mm at the inlet and 80 × 80 mm at the outlet with a 150 mm length and 5 mm thickness of mild steel material, and vice versa for the rear part of the EHE. The middle part of the EHE was a square duct with a cross-section of 80 × 80 mm, thickness of 3 mm, and length of 300 mm. All parts of the exhaust heat exchanger were fastened with flanges of mild steel material.

Numerical Formulation

As per the simulation model description and geometry configuration, a three-dimensional (3D) numerical model was constructed using ANSYS FLUENT- 18.2, and the finite volume method (FVM) was used for discretization. The equations of continuity, momentum, and energy were the governing equations for the simulation of the exhaust heat exchanger.

The continuity equation state that

$$\frac{\partial \rho}{\partial t} + \nabla \cdot (\rho \vec{V}) = 0 \quad (2)$$

Where, ρ represents density, $\vec{V} = (u, v, \omega)$ represents the velocity vector, and t indicates time.

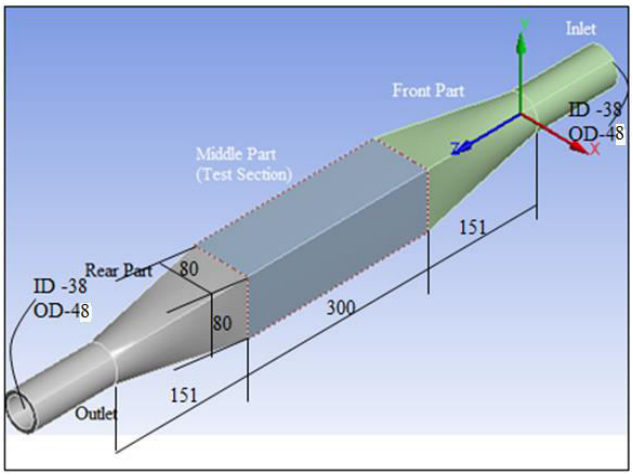

Figure-4. 3D model of the exhaust heat exchanger.

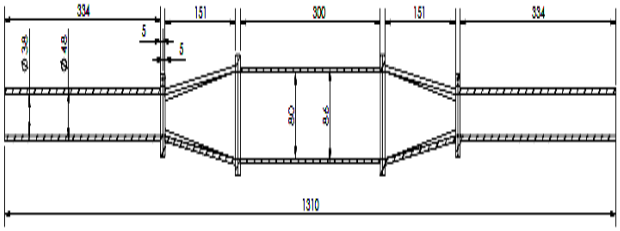

Figure-5. Schematic layout of exhaust heat exchanger (test section 80 × 80 × 300 mm).

The momentum equations for Cartesian coordinate are

$$\frac{\partial(\rho u)}{\partial t} + \nabla \cdot (u \rho \vec{V}) = -\frac{\partial P}{\partial x} + \nabla \cdot (\mu \nabla u) + X \quad (3)$$

$$\frac{\partial(\rho v)}{\partial t} + \nabla \cdot (v \rho \vec{V}) = -\frac{\partial P}{\partial y} + \nabla \cdot (\mu \nabla v) + Y \quad (4)$$

$$\frac{\partial(\rho \omega)}{\partial t} + \nabla \cdot (\omega \rho \vec{V}) = -\frac{\partial P}{\partial z} + \nabla \cdot (\mu \nabla \omega) + Z \quad (5)$$

Where, X , Y , Z represent forces per unit volume in x, y , and z components. μ indicates viscosity of the fluid and P is the pressure.

The energy equation is

$$\rho C_P \left(u \frac{\partial T}{\partial x} + v \frac{\partial T}{\partial y} + \omega \frac{\partial T}{\partial z} \right) = k \left(\frac{\partial^2 T}{\partial x^2} + \frac{\partial^2 T}{\partial y^2} + \frac{\partial^2 T}{\partial z^2} \right) + \mu \varphi + \dot{q} \quad (6)$$

Where, $\mu\varphi$ and $\dot{q}$ indicate viscous dissipation and volumetric rate of thermal energy generation, respectively. T indicates the temperature, C_P represents the specific heat at constant pressure and k indicates the thermal conductivity.

Note: The energy of the fluid per unit mass is $e_{stream} = h = C_p T$

BOUNDARY CONDITIONS

A single-cylinder four-stroke, constant speed diesel engine was used in this study. According to the engine performance, an engine exhaust flow rate of 0.0082 kg/s and temperature of 280.5°C were obtained when the engine was running at a full load condition of 10 kg with an engine speed of 1500 rpm. For an incompressible fluid, either the velocity or the mass flow rate can be used as the inlet boundary condition. Therefore, the mass flow rate of the engine exhaust was set to 0.0082 kg/s and the engine exhaust temperature was set to 280.5°C. The engine exhaust was released into the atmosphere; therefore, the exhaust pressure at the outlet of the EHE was approximately the typical atmospheric pressure, that is, the gauge pressure at the outlet was set to zero Pa. In addition, the coefficient of heat transfer between the outside surface of the test section and atmospheric air was set to 20 W/m^2 K, with the environment (air) temperature set to 28°C. The engine exhaust was considered to be fair, the characteristics of which change with temperature. Aluminum and mild steel materials of the test section and the remaining parts of the exhaust heat exchanger were employed, respectively. For this simulation, the standard equations of $K-\varepsilon$ were adopted as the turbulence models. The model assumes that the viscosity can be ignored. The no-slip boundary conditions were applied to all solid walls. The governing equations, such as the continuity equation, momentum equation and energy equation were included using the first-order upwind discrete method, and other parameters were set as the system default. The working fluid was considered to be in a steady state and incompressible, and the density was assumed to be constant.

MESH TEST

Prior to the parametric study, a mesh test was conducted to confirm the numerical results. The numerical simulations were performed until the results were complete. The computational domain is meshed using unstructured tetrahedral elements. Grid or mesh convergence is the term used to describe the development of results using smaller cell sizes for the calculations. The numerical solution provided by a computational model tends to a unique value as the mesh density increases. Computer systems are required to perform the simulation. A mesh test should be performed to determine the appropriate mesh size for use in different cases of the exhaust system. Therefore, CFD analysis was initially performed on an aluminum test section of 80 × 80 × 300 mm with a thickness of 3 mm. Different mesh sizes, such as 5, 3, 2, 1.5 and 1 mm were used to verify the mesh convergence. The mesh size of the test section was maintained at 5, 3, 2, 1.5, and 1 mm and inflation were applied along its boundary. Figures 6-10 show the meshing size and the respective simulation results of the surface temperature field on the test section. The element counts for this mesh generated were 0.6, 1.4, 4, 9.7 and 32.2 million elements or cell counts respectively. The maximum temperatures observed on the aluminum test section of the exhaust heat exchanger at different mesh sizes, that is, 5, 3, 2, 1.5 and 1 mm, were 156.20, 166.71, 172.97, 173.54 and 173.62°C respectively. The mesh size 1.5 mm and 1 mm showed the same maximum surface temperature; however, the run time of the 1 mm mesh size was greater. Hence, a mesh size of 1.5 mm was selected, as it gave the best result and did not obstruct the accuracy of the analysis. The mesh size with the number of elements/cells counts and the maximum temperature are shown in Figure-11. The surface temperature distribution on the test section of the exhaust heat exchanger using a 1.5 mm mesh size is shown in Figure-12.

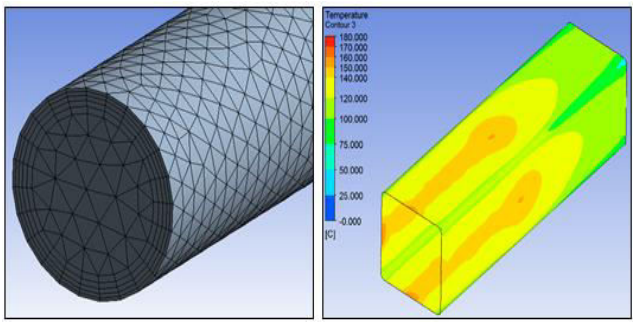

Figure-6. Mesh size of 5 mm and simulation result of temperature field/distribution on test section (80×80×300) by using 5 mm mesh size.

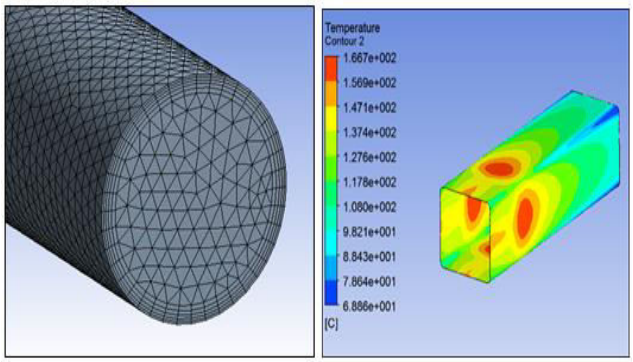

Figure-7. Mesh size of 3 mm and simulation result of temperature field/distribution on test section (80×80×300) by using 3 mm mesh size.

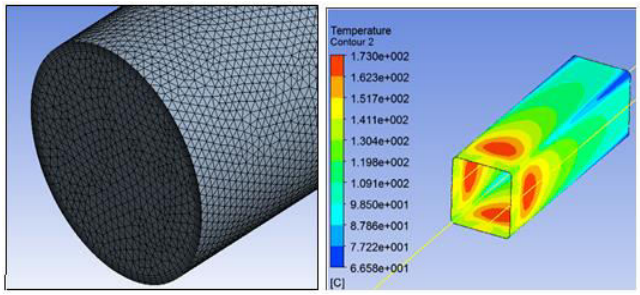

Figure-8. Mesh size of 2 mm and simulation result of temperature field/distribution on test section (80×80×300) by using 2 mm mesh size.

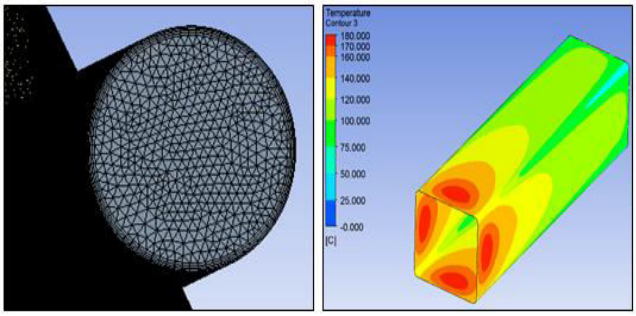

Figure-9. Mesh size of 1.5 mm and simulation result of temperature field/distribution on test section (80×80×300) by using 1.5 mm mesh size.

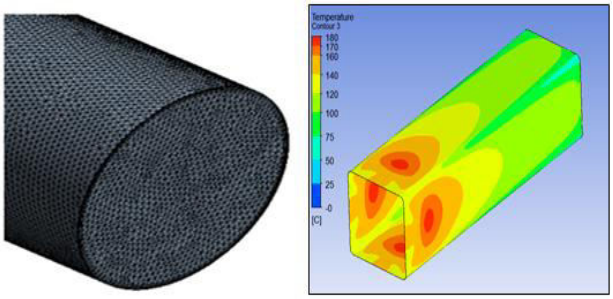

Figure-10. Mesh size of 1 mm and simulation result of temperature field/distribution on test section (80×80×300) by using 1 mm mesh size.

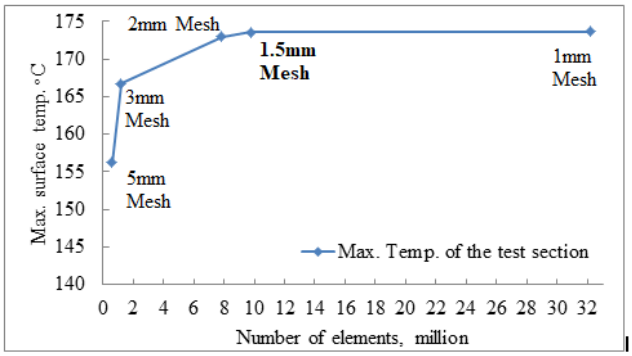

Figure-11. Variation of maximum surface temperature with cell count.

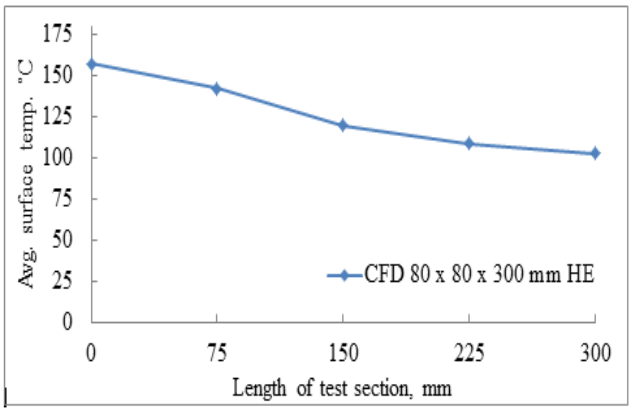

Figure-12. Temperature distributions on the test section of 80 × 80 × 300 mm by using 1.5 mm mesh size.

THERMAL ANALYSIS

The numerical simulation result of the thermal field of the test section (80 mm × 80 mm × 300 mm) using a 1.5 mm mesh size is shown in Figure-9. The distribution of the surface temperature along the length of the test section (1.5 mm mesh size) is graphically represented in Figure-12.

According to the simulation results of the test section, a maximum temperature of 157°C was obtained at the beginning and gradually decreased with increasing length of the test section. At the outlet of the test section, a temperature of 102.25°C was obtained.

The temperature uniformity coefficient has been calculated using Equation 1. In this case, the temperature uniformity is 0.67. The temperature uniformity coefficient indicates the temperature distribution. To improve the surface temperature and temperature uniformity coefficient, it is necessary to investigate the test sections of the exhaust heat exchangers with different dimensions and inserts.

EXPERIMENTAL AND SIMULATION RESULT VALIDATION

The simulation and experimental results of the test section of 80 mm × 80mm × 300 mm were compared in terms of the heat transfer coefficient shown in Figure-13. It was observed that the heat transfer coefficient of the CFD analysis was high at the inlet of the test section of the exhaust heat exchanger; however, it was closer to each other with the length of the test section.

At the outlet of the test section, there was a small difference between the theoretical and experimental heat transfer coefficients. A maximum error of 20% was observed at the inlet of the test section, and a minimum error of 6.1% at the length of the test section of 75 mm.

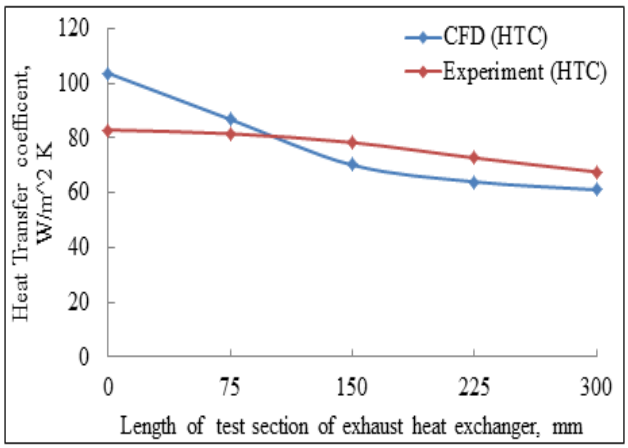

Figure-13. Comparison of numerical and experimental results of the test section of 80 × 80 × 300 mm.

TEST SECTION GEOMETRY

Generally, thermoelectric module sizes of 30 × 30 to 60 × 60 mm with thicknesses of 3 - 5 mm are available. Therefore, the test section of the exhaust heat exchanger should have a minimum width of 60 mm, with a suitable length that depends on the available heat, space, thermoelectric module size and use quantity. This type of heat exchanger can be used for all sizes of thermoelectric modules with different thicknesses. For this reason, different sizes of test sections were studied in this study, as shown in Table-1.

Table-1. Different types of test section with dimensions.

S. No.	Type of test section	Size of test section (width × height × length) mm
1	A-type	80 × 80 × 300
2	B-type	80 × 80 × 240
3	C-type	80 × 80 × 180
4	D-type	60 × 60 × 300
5	E-type	60 × 60 × 240
6	F-type	60 × 60 × 180
7	G-type	60 × 60 × 180 with cone type insert
8	H-type	60 × 60 × 180 with cone-cylinder type insert
9	I-Type	60 × 60 × 180 with cone-cylinder-cone type insert

Schematic Layout of the Exhaust Heat Exchanger

The schematic layout of the exhaust heat exchangers with having A-type, B-type, and C-type test sections are shown in Figures 14, 15, and 16, respectively. The A-type, B-type, and C-type test sections of the exhaust heat exchanger had the same cross-sectional area of 80 × 80 mm with different lengths of 300, 240, and 180 mm. The cross-sectional areas of the test sections were reduced to 60 × 60 mm each with the same lengths of 300, 240, and 180 mm and are called D-type, E-type, and F-type test sections, respectively, as shown in Figures 17, 18, and 19. Different types of inserts were used to improve the performance of the heat exchanger (EHE). The inserts of the cone type, cylinder-cone type, and cone-cylinder-cone type were inserted in the test section of the EHE to direct the exhaust flow for developing extreme performance of the heat exchangers, as shown in Figures 20, 21, and 22, which are called G-type, H-type, and I-type test sections, respectively. The G-type test section has a cone-type insert with a 46.5 mm base diameter and 180 mm length. The cylinder-cone type insert is used in the H-type test section having 46.5 mm base diameter with 90 mm length of cone and 46.5 mm diameter with 90 mm length of cylinder.

The I-type test section has a cone-cylinder-cone type insert with a 46.5 mm base diameter and 100 mm length cones on both sides of the cylinder with a46.5 mm diameter and 180 mm length. All types of inserts were inserted into 60 mm × 60 mm × 180 mm test sections of the exhaust heat exchanger.

RESULTS AND DISCUSSIONS

After validating the simulation results with the experimental results, the simulation model of the EHE can be used for parametric analysis of the EHE, which is the main element of the TEG. Based on the TEM size, quantity and available space, parametric analysis should be performed using simulation models to reduce time and cost. The same initial boundary conditions and assumptions were applied for the parametric analysis.

Temperature Distribution

The simulation model was used to determine the surface temperature field/distribution for all test sections (A - I) of the EHE. The temperature distributions of the A, B and C-type test sections are shown in Figures 23, 24, and 25 respectively. Figure-26 shows the temperature plots of the A, B and C-type test sections. The temperature distribution and its plots indicate that the A, B, and C-type test sections have temperature ranges of 102.25 - 157.00, 107.26 - 157.48 and 111.28 - 168.56^{o}C respectively. The temperature ranges slightly, owing to the reduction in the length of the test section. The C-type test section exhibited a more uniform temperature distribution than the A and B-type test sections.

The temperature distributions of the D, E, and F-type test sections were simulated using CFD tools, as shown in Figures 27, 28, and 29, respectively. The temperature plot of the test sections of types D, E, and F-type are graphically represented in figure 30. Based on the temperature distribution and their plots, it was observed that the test sections of D, E and F-type have temperatures range of 126.34 - 158.28, 128.68 - 157.78 and 130.59 - 160.24^{o}C respectively. The F-type test section of the exhaust heat exchanger has a higher surface temperature with a uniform distribution than the other test sections such as A, B, C, D, and E-type.

The performance of the F-type test section can be improved using different types of inserts to increase the surface temperature and its distribution. Different types of inserts such as cone, cylinder-cone, and cone-cylinder-cone, are used in the F-type test sections called G, H, and I-type test sections, respectively.

The temperature field/distributions are shown in Figures 31, 32, and 33. Figure-34 shows the temperature plots of the G, H, and I-type test sections. The G, H, and I-type test sections show a temperature range of 153.27 - 161.64, 158.86 - 162.09 and 154.78 - 180.00^{o}C respectively. The H-type test section had more temperature uniformity than the G and I-type sections.

Pressure Drop

This pressure drop can reduce the efficiency of the heat source. Therefore, a minimum pressure drop should be created by the heat exchanger, with or without inserts. The pressure drops created by the A, B, and C-type test sections are shown in Figure-35.

Figure-36 shows the pressure drop plots for the D, E, and F-type test sections. The test section with inserts, such as G, H and I type test section creates a pressure drop on the heat source, as shown in Figure-37.

According to the pressure drop plots, test sections A, B, and C-type show a pressure drop in the range of 51.3 - 51.6 Pa. The D, E and F-type test sections create pressure drops in the range of 52.1 - 52.6 Pa, slightly more than A, B and C-type test sections because they are reduced in the cross-section area of the test sections.

The G, H and I-type test sections with inserts show maximum pressure drops of 71.8, 72.2 and 82.1 Pa respectively. The inserts reduced the flow area of the test section, which increased the pressure drop in the test section of the exhaust heat exchanger system.

Fluid Velocity

Figure-38 shows the velocity plots of the C-type and F-type test sections of the EHE. The exhaust velocity depends on the engine exhaust flow rate and geometry of the test section. The results show that the cross sect of 80 mm × 80 mm with a length of 180 mm (C-type) test section shows an exhaust velocity range of 2.00 - 2.77 m/s and a cross section of 60 mm × 60 mm with a length of 180 mm (F-type) test section shows an exhaust velocity range of 3.40 - 3.73 m/s.

The density of the engine exhaust was constant so that the exhaust velocity was inversely proportional to the cross-section of the test section.

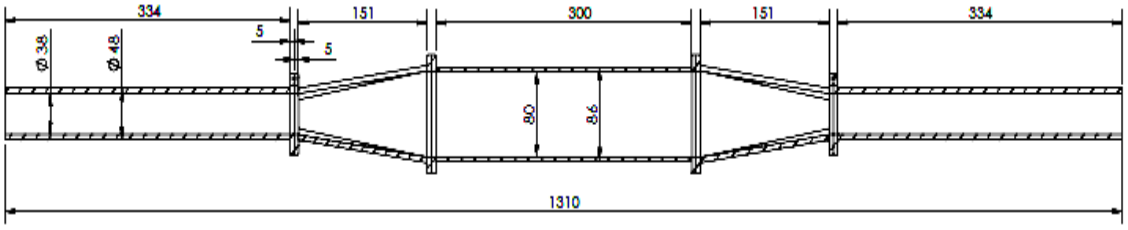

Figure-14. Schematic layout of exhaust heat exchanger (test section 80 × 80 × 300 mm) (A-type).

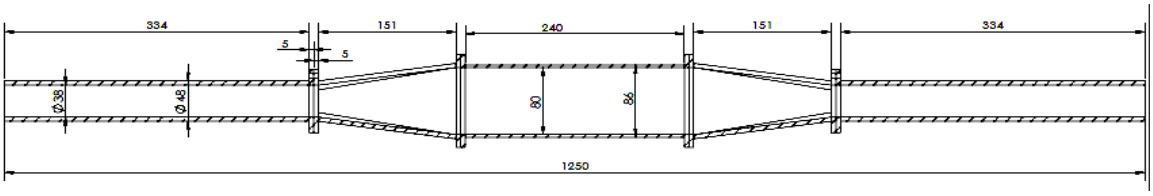

Figure-15. Schematic layout of exhaust heat exchanger (test section 80 × 80 × 240 mm) (B-type).

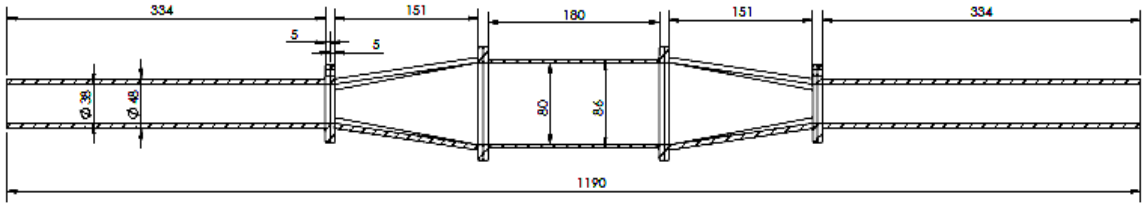

Figure-16. Schematic layout of exhaust heat exchanger (test section 80 × 80 × 180 mm) (C-type).

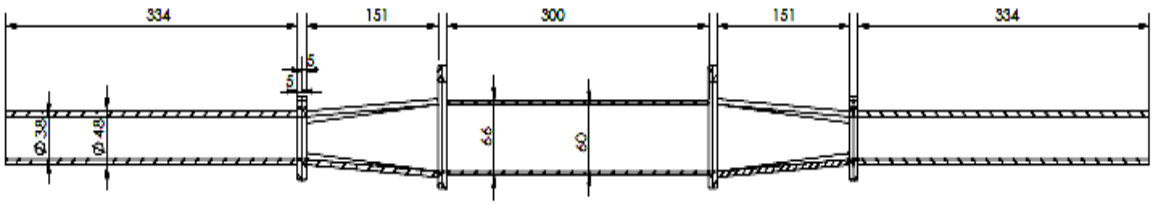

Figure-17. Schematic layout of exhaust heat exchanger (test section 60 × 60 × 300 mm) (D-type).

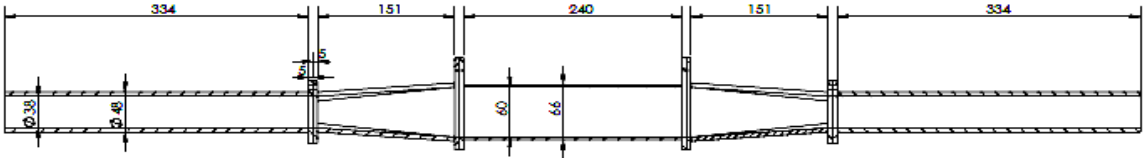

Figure-18. Schematic layout of exhaust heat exchanger (test section 60 × 60 × 240 mm) (E-type).

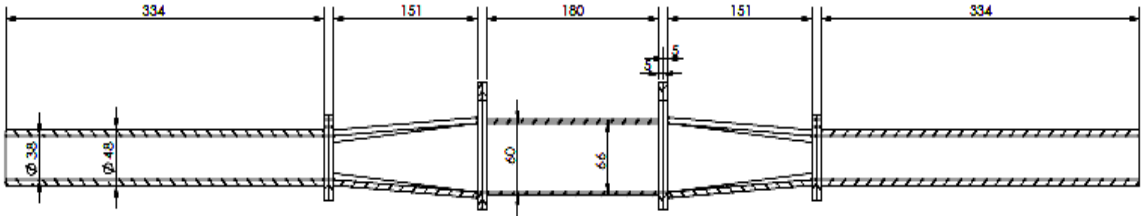

Figure-19. Schematic layout of exhaust heat exchanger (test section 60 × 60 × 180 mm) (F-type).

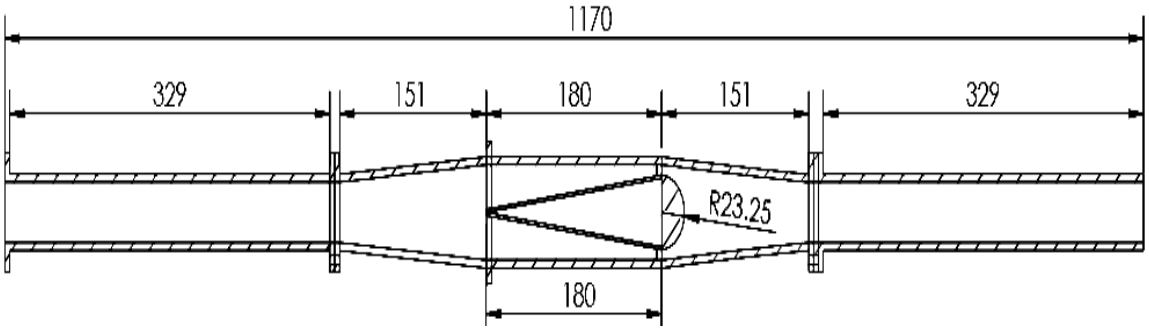

Figure-20. Schematic layout of exhaust heat exchanger (test section 60 × 60 × 180 mm) with cone-insert (G-type).

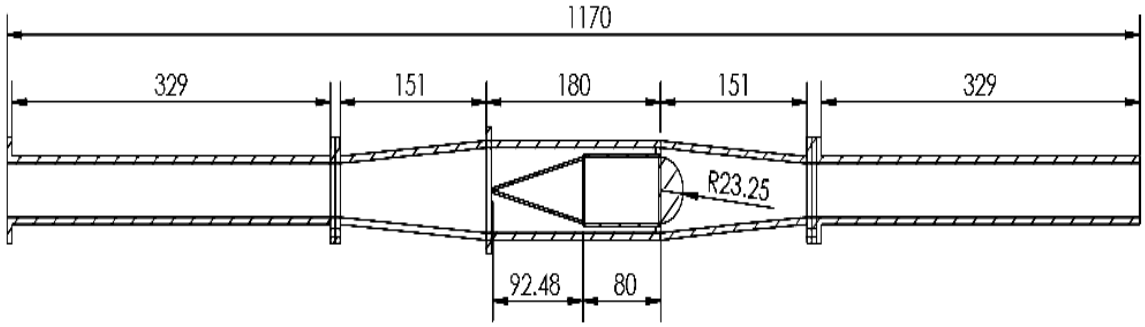

Figure-21. Schematic layout of exhaust heat exchanger (test section 60 × 60 × 180 mm) with cone-cylinder insert (H-type).

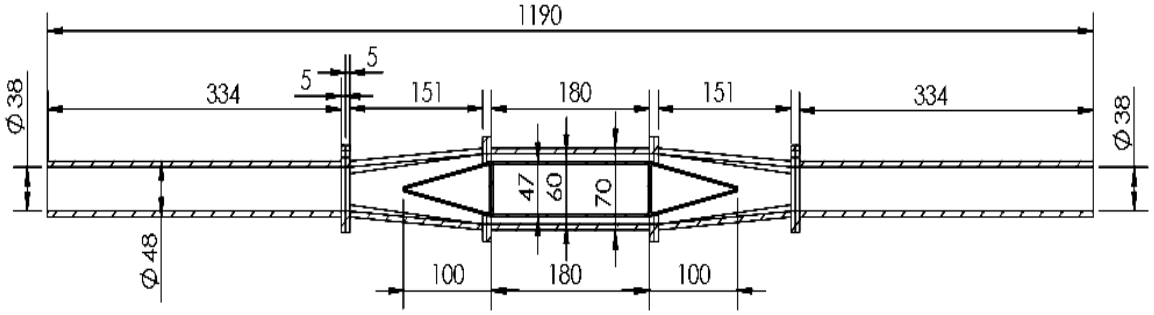

Figure-22. Schematic layout of exhaust heat exchanger (test section 60 × 60 × 180 mm) with cone-cylinder-cone insert (I-type).

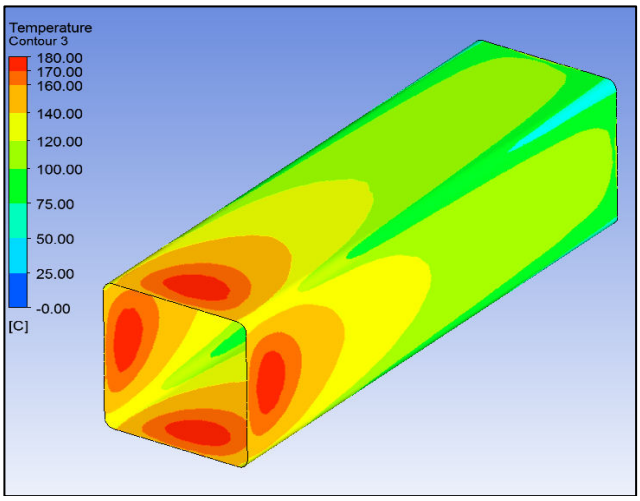

Figure-23. Simulation result of temperature field on test section (80×80×300) (A-type).

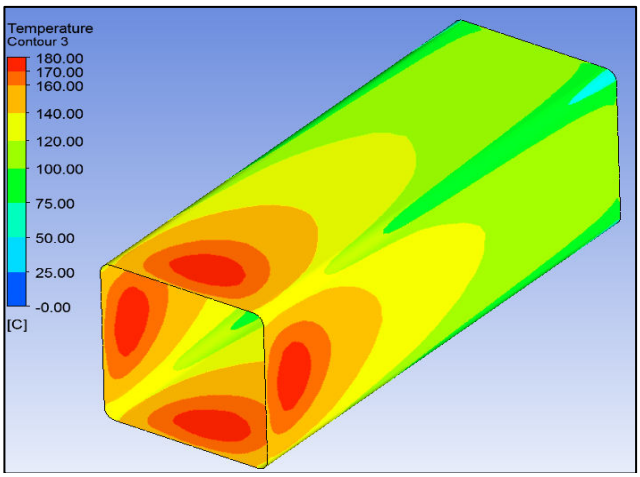

Figure-24. Simulation result of temperature field on test section (80×80×240) (B-type).

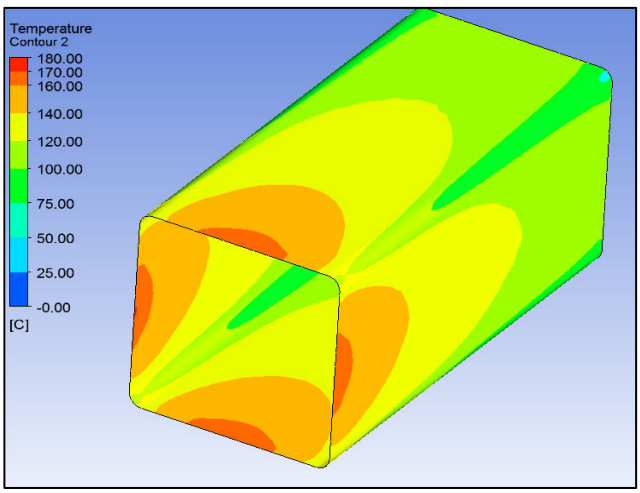

Figure-25. Simulation result of temperature field on test section (80×80×180) (C-type).

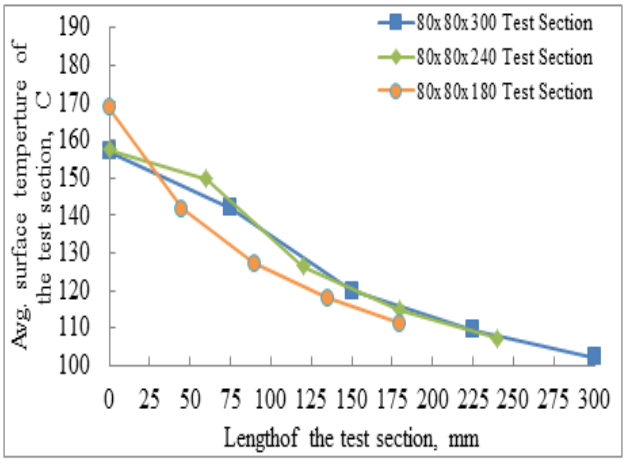

Figure-26. Temperature plots of test sections (80×80×300-240-180) (A, B, C-type).

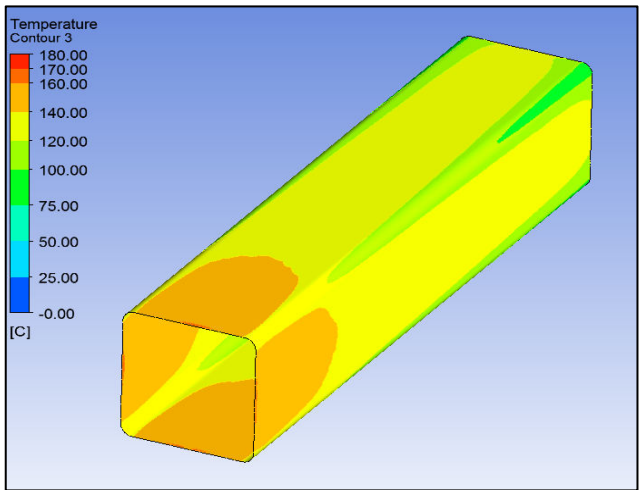

Figure-27. Simulation result of temperature field on test section (60×60×300) (D-type).

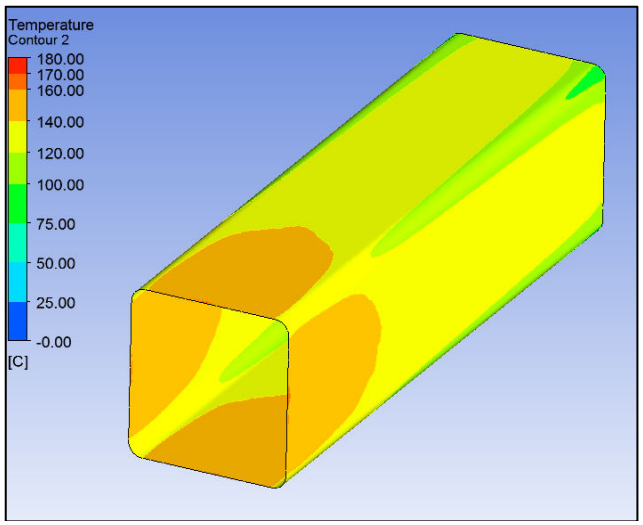

Figure-28. Simulation result of temperature field on test section (60×60×240) (E-type).

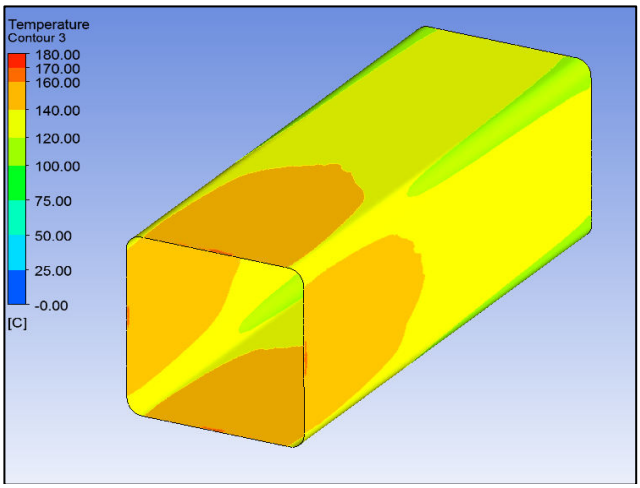

Figure-29. Simulation result of temperature field on test section (60×60×180) (D-type).

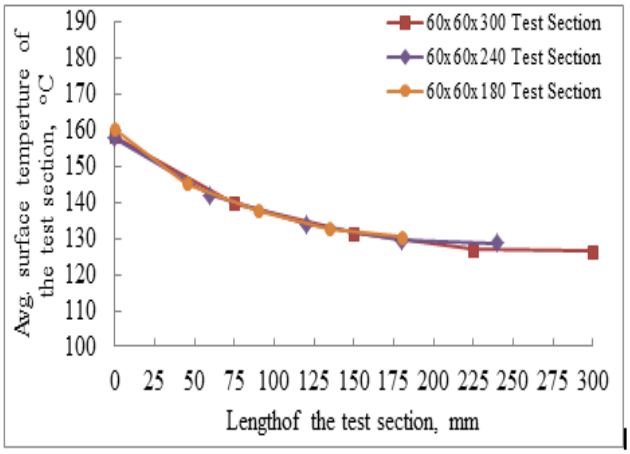

Figure-30. Temperature plots of test sections (60×60×300-240-180) (D, E, F-type).

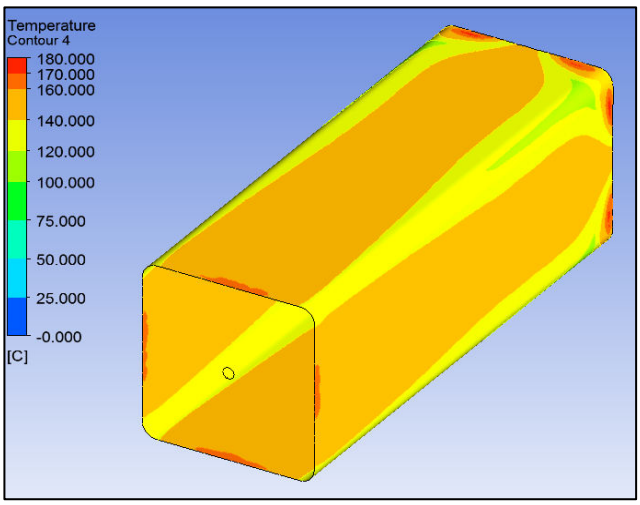

Figure-31. Simulation result of temperature field/ on test section (60×60×180) with Cone type insert (G-type).

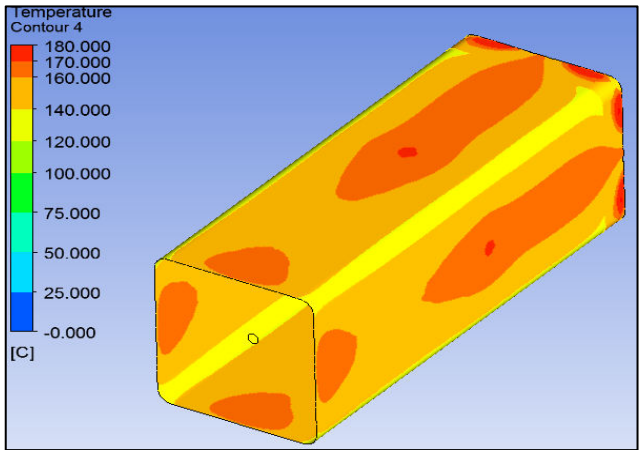

Figure-32. Simulation result of temperature field on test section (60×60×180) with Cylinder-Cone type insert (H-type).

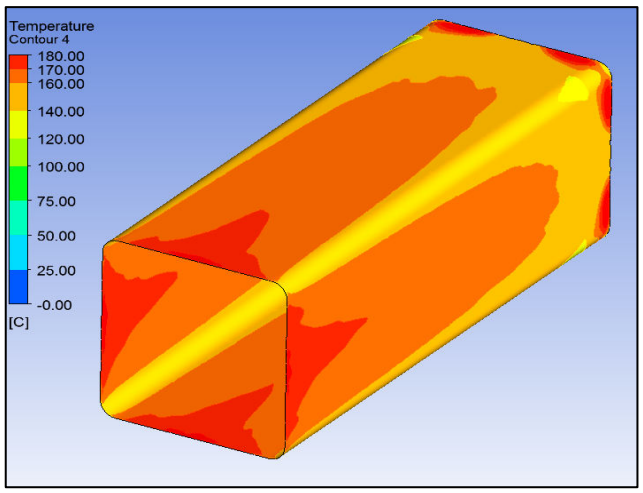

Figure-33. Simulation result of temperature field on test section (60×60×180) with Cone-Cylinder-Cone type insert (I-type).

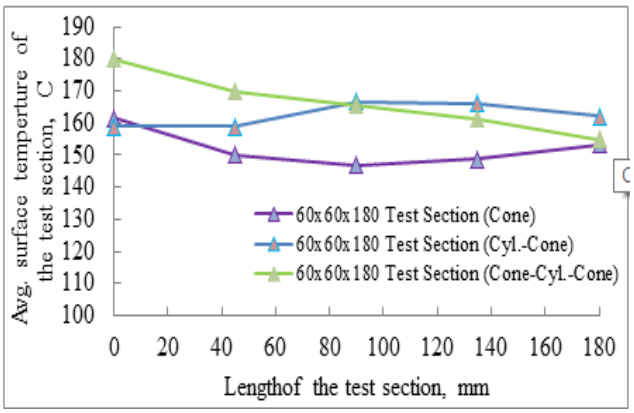

Figure-34. Temperature plots of test sections (80×80×180 mm with inserts) (G, H, I-type)

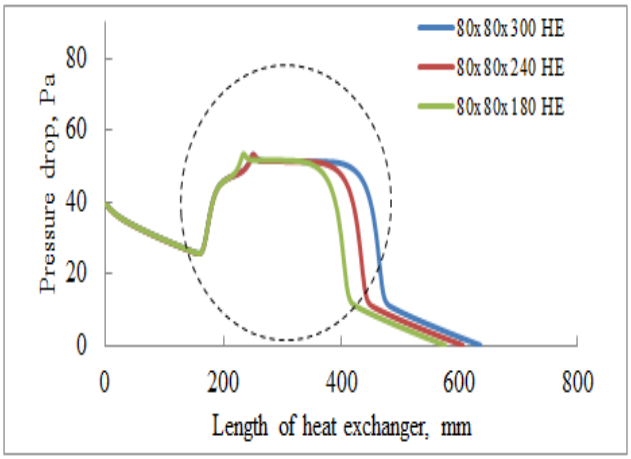

Figure-35. Pressure drop plot of heat exchangers (test section of 80×80×300-240-180 mm) (A, B, C-type).

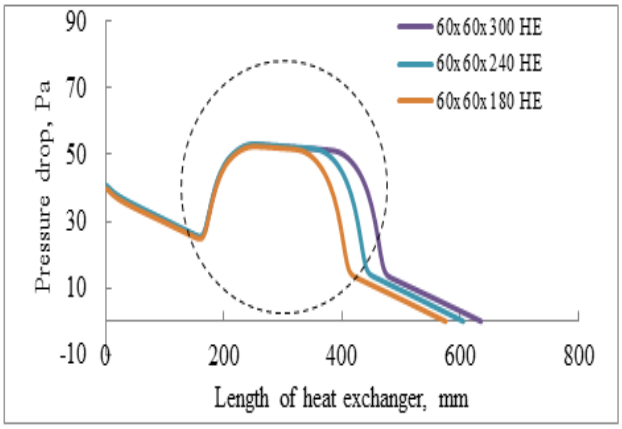

Figure-36. Pressure drop plot of heat exchangers (test section of 60×60×300-240-180 mm) (D, E, F-type).

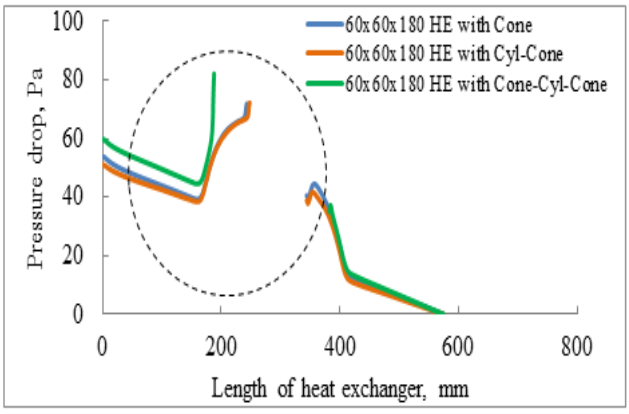

Figure-37. Pressure drop plot of heat exchangers (test section of 60×60×180 mm with inserts) (G, H, I-type).

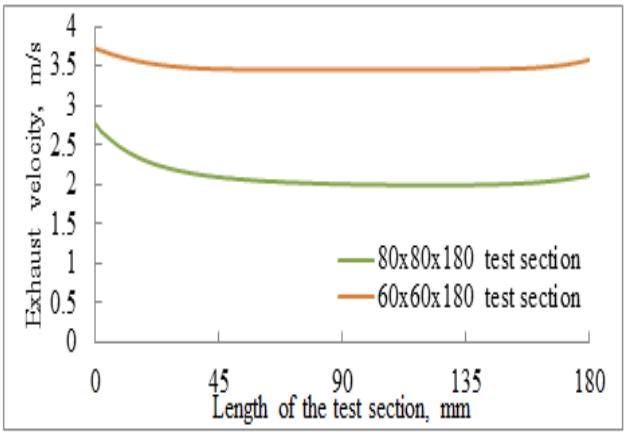

Figure-38. Velocity plot of test section (80×80×180 mm and 60×60×180 mm) (C, F-type).

The heat transfer rate increased with the exhaust velocity. A test section with high fluid velocity is preferred as a heat source for the TEG for power generation. According to the velocity plot of the C-type and F-type test section of the exhaust heat exchanger, it was observed that the higher the exhaust velocity at the entry and exit of the test section higher than that at the middle section. A constant exhaust velocity was revealed in the middle section of the test section.

Temperature Uniformity

Temperature uniformity is as important as the surface temperature of the test section of the exhaust heat exchanger. A non-uniform temperature distribution creates thermal stresses in the test section to make rough contact at the interface of the test section and the thermoelectric module. The temperature uniformity was measured in terms of the temperature uniformity coefficient. Therefore, the temperature uniformity coefficient should be determined for all test sections of the heat exchanger.

The thermal uniform coefficients of all the test sections are graphically represented in Figure-39. Equation (1) was used to determine the temperature uniformity coefficients of the test sections. It was observed that the A, B, and C-type test sections showed very low-temperature uniformity coefficients of 0.67, 0.69, and 0.71, respectively. The test sections of D, E and F-type showed 0.84, 0.85 and 0.86 temperature uniformity coefficients respectively, but this was not sufficient.

The G, H and I-type test sections show high temperature uniformity coefficients of 0.94, 096, and 0.91, respectively. The cone-type, cylinder-cone-type and cone-cylinder-cone-type inserts were used to improve not only the surface temperature but also the temperature uniformity coefficient of the test sections.

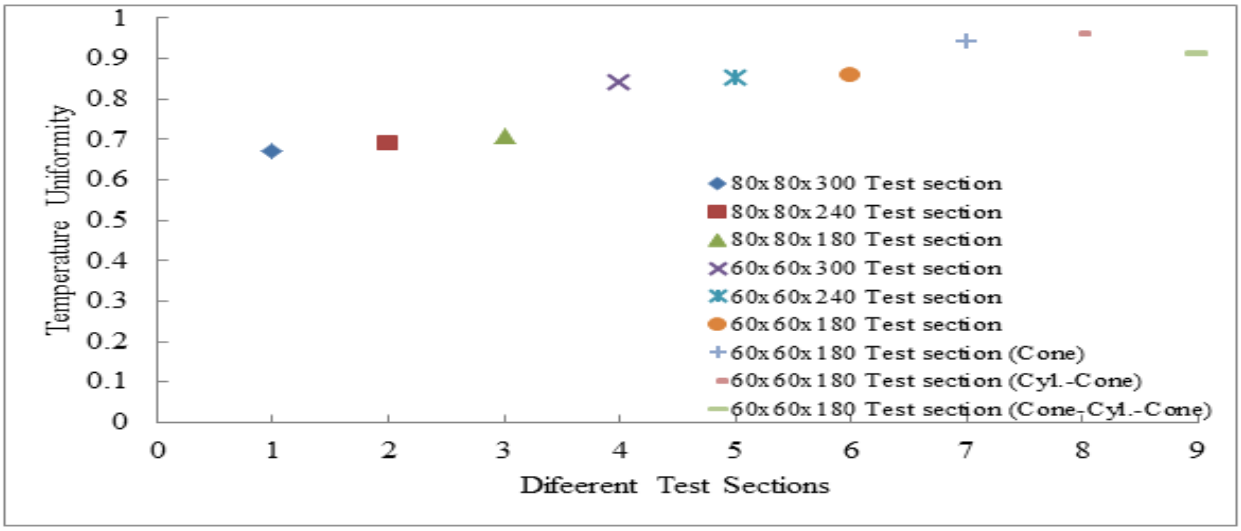

Figure-39. Temperature uniformity coefficients of all test sections (A to I-type).

CONCLUSIONS

Experiments were performed on an 80 mm × 80 mm × 300 mm test section of the exhaust heat exchanger under specific operating conditions. The simulation tool computational fluid dynamics simulation tool was used to determine the performance of the 80 mm × 80 mm ×300 mm test section. The simulation results were validated with experimental results to ensure the performance of the simulation model. A simulation model with a 1.5 mm mesh size was used to determine the temperature distribution, temperature uniformity, fluid velocity and pressure drop of the exhaust heat exchanger with different types of test sections. The test section of 60 mm × 60 mm × 180 mm (F-type) shows a higher surface temperature with an allowable pressure drop than the other types of test sections without inserts. It was observed that the surface temperature gradually declined with the increasing length of the test section. The inserts played a vital role in enhancing the surface temperature distribution and uniformity coefficient. The Cone type, Cone-Cylinder type and Cone-Cylinder-Cone type inserts are used to improve the performance of the F-type test section. The inserts used in the F-type test section were G-type, H-type and I-type test sections. The results indicate that the G and H-type test sections of the exhaust heat exchanger have a high surface temperature and high temperature uniformity with an allowable pressure drop. The G-type and H-type test sections of the heat exchanger can be used for thermoelectric generators to produce electric power. This work aids in the design of thermo-electric generator systems. In the future, different types of insert geometries should be designed with an allowable pressure drop to enhance the heat transfer coefficient of the heat exchanger used in thermoelectric generators.

ACKNOWLEDGEMENTS:

The authors acknowledge the management of G H Raisoni College of Engineering and Management, Wagholi, Pune, India for providing a research laboratory for the research and their support of this work.

FUNDING:

Not applicable

CONFLICT OF INTEREST:

The authors declare that they have no known competing financial interests or personal relationships that could have appeared to influence the work reported in this research paper.

REFERENCES

Amaral Calil, Brandao Caio, Sempels Éric V., Lesage Frederic J. 2014. Net thermoelectric generator power output using inner channel geometries with alternating flow impeding panels. Applied Thermal Engineering. 65: 94-101.
https://doi.org/10.1016/j.applthermaleng.2013.12.044

Bai Shengqiang, Lu Hongliang, Wu Ting, Yin Xianglin, Shi Xun, Chen Lidong. 2014. Numerical and experimental analysis for exhaust heat exchangers in automobile thermoelectric generators. Case Studies in Thermal Engineering. 4: 99-112.
https://doi.org/10.1016/j.csite.2014.07.003

Deng Y. D., Liu X., Chen S., Tong N. Q. 2013. Thermal Optimization of the Heat Exchanger in an Automotive Exhaust-Based Thermoelectric Generator. Journal of Electronic Materials. 42(7): 1334-1340.
https://link.springer.com/article/10.1007/s11664-012-2359-0

Kim Tae Young, Lee Seokhwan, Lee Janghee. 2016. Fabrication of thermoelectric modules and heat transfer analysis on internal plate fin structures of a thermoelectric generator. Energy Conversion and Management. 124: 470-479.
https://doi.org/10.1016/j.enconman.2016.07.040

Kumar C. Ramesh, Sonthalia Ankit, Goel Rahul. 2011. Experimental Study on Waste Heat Recovery from an Internal Combustion Engine using Thermoelectric Technology Thermal Science. 15(4): 1011-1022. http://www.doiserbia.nb.rs/img/doi/0354-9836/2011/0354-98361100053K.pdf

Liu X., Deng Y. D., Zhang K., Xu M., Xu Y., Su C. Q. 2014. Experiments and simulations on heat exchangers in thermoelectric generator for automotive application. Applied Thermal Engineering. 71: 364-370. https://doi.org/10.1016/j.applthermaleng.2014.07.022

Liu X., Deng Y. D., Chen S., Wang W.S., Xu Y., Su C. Q. 2014. A case study on compatibility of automotive exhaust thermoelectric Generation system, catalytic converter and muffler. Case Studies in Thermal Engineering. 2: 62-66. https://www.sciencedirect.com/science/article/pii/S2214157X14000033

Patil Dipak S., Arakerimath Rachayya R., Walke Pramod V. 2018. Experimental investigation and optimization of a low-temperature thermoelectric module with different operating conditions. World Journal of Engineering. 16(3): 1-10. https://doi.org/10.1108/WJE-07-2018-0248

Patil Dipak S., Rachayya Arakerimath R., Walke Pramod V. 2018. Thermoelectric materials and heat exchangers for power generation – A review. Renewable and Sustainable Energy Reviews. 95: 1-22. https://doi.org/10.1016/j.rser.2018.07.003

Su C.Q., Wang W. S., Liu X., Deng Y. D. 2014. Simulation and experimental study on thermal optimization of the heat exchanger for automotive exhaust-based Thermoelectric generators. Case Studies in Thermal Engineering. 4: 85-91. https://doi.org/10.1016/j.csite.2014.06.002

Su C. Q., Zhan W. W., Shen S. 2012. Thermal Optimization of the Heat Exchanger in the Vehicular Waste-Heat Thermoelectric Generations. Journal of Electronic Materials. 41(6): 1693-1697. https://link.springer.com/article/10.1007/s11664-012-2359-0

Su C. Q., Wang W. S., Liu X., Deng Y. D. 2014 Simulation and experimental study on thermal optimization of the heat exchanger for automotive exhaust-based Thermoelectric generators. Case Studies in Thermal Engineering. 4: 85-91. https://doi.org/10.1016/j.csite.2014.06.002

Tang Z. B., Y. Deng D., Su C.Q., Yuan X. H. 2015. Fluid Analysis and Improved Structure of an ATEG Heat Exchanger Based on Computational Fluid Dynamics. Journal of Electronic Materials. 44: 1554-1561. https://link.springer.com/article/10.1007/s11664-014-3472-z

Tzeng Sheng-Chung, Jeng Tzer-Ming, Lin Yi-Liang. 2014. Parametric study of heat-transfer design on the thermoelectric generator system. International Communications in Heat and Mass Transfer. 52: 97-105. https://doi.org/10.1016/j.icheatmasstransfer.2014.01.021

Weng Chien-Chou, Huang Mei-Jiau. 2013. A simulation study of automotive waste heat recovery using a thermoelectric power generator. International Journal of Thermal Sciences. 71: 302-309. https://doi.org/10.1016/j.ijthermalsci.2013.04.008

Wang Tongcai, Luan Weiling, Wang Wei, Tu Shan-Tung. 2014. Waste heat recovery through plate heat exchanger based thermoelectric generator system. Applied Energy. 136: 860-865. https://doi.org/10.1016/j.apenergy.2014.07.083

Wang Yiping, Li Shuai, Yang Xue, Deng Yadong, Su Chuqi. 2016. Numerical and Experimental Investigation for Heat Transfer Enhancement by Dimpled Surface Heat Exchanger in Thermoelectric Generator. Journal of Electronic Materials. 45(3): 1792-1802. https://link.springer.com/article/10.1007/s11664-015-4228-0